Fourth International Symposium on Marine Propulsors
smp'15, Austin, Texas, USA, June 2015

Influence of the Numerical Propulsion Modelling on the Velocity Distribution behind the Propulsion Device and Manoeuvring Forces

*Jan Clemens Neitzel[1], Markus Pergande[1], Stephan Berger[1], Moustafa Abdel-Maksoud[1]

[1]Institute for Fluid Dynamics and Ship Theory, Hamburg University of Technology (TUHH), Hamburg, Germany

*Corresponding author: jan.neitzel@tuhh.de

Abstract

The influence of different propulsor modelling approaches on manoeuvring simulations and rudder forces is analysed. In the numerical study, the RANS solver ANSYS CFX is employed. Three approaches for modelling the propulsor are investigated: a fully modelled propeller, a coupled simulation with a potential flow solver and an actuator disk. For the validation, open water and captive model test results are used.

1 Introduction

The numerical investigation of ship manoeuvres with RANS methods often causes a huge computational effort. In order to accurately capture relevant effects as for example propeller and rudder forces or the influence of the free water surface, a relatively fine discretisation with respect to space and time is required. A considerable percentage of the computational effort is due to modelling the propeller in a geometrically resolved manner.

Therefore, the development of different modelling techniques to consider the influence of the propulsion unit on the flow is required for time-efficient simulations. In RANS simulations, the propeller can be included as a fully modelled propeller or by applying the body-force technique. The calculation of the body force distribution can be based on coupling with a boundary element method or using an actuator disk model.

The fully resolved propeller is a common method to simulate the propulsor either in open water condition or behind a ship hull. Greve et al. (2010) contributed a study on the general forces acting on the ship under propulsion test condition. Bugalski et al. (2011) demonstrate a good accordance of the experimental and numerical results for the MOERI KCS container ship. A detailed study of the effects of the fully modelled propeller on the flow behaviour behind the propulsor is done by Krasilnikov (2013).

Coupling a viscous method for the outer flow with an inviscid boundary element method (BEM) permits the consideration of the local forces generated by the blades as shown by Wöckner et al (2011). Rijpkema et al. (2013) examined the behaviour of the propulsor behind a ship hull with a RANS-BEM. The application of the BEM coupling algorithm displays a slight error of 2 to 3% in comparison to experimental data.

Krasilnikov (2013) furthermore investigated the influence of an actuator disk for the simulation of the propeller. Concluding on a good agreement, the advantage of a significantly lower amount of computational effort is emphasized. With regard to work done by Soukup (2008) and Xing-Kaeding (2006) the actuator disk model can be seen as a reasonable alternative for propulsor modelling.

The following paper focuses on the interaction of propeller, hull and rudder for the three mentioned modelling techniques. The applicability of the numerical fluid dynamics calculations is investigated and the results of the simulations are compared to model test results. Therefore, the forces acting on the propeller, hull and rudder are calculated and the velocity distribution behind the propeller is analysed.

2 Propulsor modelling

2.1 Boundary element method coupling

The RANS-BEM coupling for *ANSYS CFX* was implemented by Berger (2013). The coupling procedure uses the in-house potential code *pan*MARE developed at the *Institute for Fluid Dynamics and Ship Theory* at the *Hamburg University of Technology*.

*pan*MARE is a first-order potential flow solver. It is assumed that the total velocity $\mathbf{U}$ in the flow domain $\boldsymbol{\Omega}$ can be divided in a background velocity field $\mathbf{U}_\infty$ and an induced flow field $\mathbf{U}^+$. The total velocity in the global coordinate system can thus be written as:

$$\boldsymbol{U} = \boldsymbol{U}_\infty + \boldsymbol{U}^+ \qquad [1]$$

In a body-fixed coordinate system rotating with the propeller, Equation [1] is rewritten to:

$$\boldsymbol{V} = \boldsymbol{V_{mot}} + \boldsymbol{V}_\infty + \boldsymbol{V}^+ \qquad [2]$$

$\mathbf{V_{mot}}$ is the velocity due to the local body motion and the background flow is considered as $\mathbf{V}_\infty$. The induced flow field $\mathbf{V}^+$ is assumed to be incompressible and irrotational. Hence, a velocity potential $\boldsymbol{\Phi} = \boldsymbol{\Phi}(\mathbf{X},t)$ with $\mathbf{V}^+ = \nabla\boldsymbol{\Phi}$ can be introduced. $\boldsymbol{\Phi}$ is a function of position and time. The governing flow equations can be simplified to Laplace's equation for the potential $\boldsymbol{\Phi}$ and Bernoulli's equation for the pressure p:

$$\nabla^2\boldsymbol{\Phi} = 0 \qquad [3]$$

and

$$p + \frac{1}{2}\rho|\boldsymbol{V}|^2 + \rho\frac{\partial\boldsymbol{\Phi}}{\partial t} + \rho g z = p_{ref} + \frac{1}{2}\rho|\boldsymbol{V_0}|^2 \qquad [4]$$

with the reference pressure p_{ref}. For a lifting body like a propeller, the surface $S = \partial\boldsymbol{\Omega}$ is divided into the blade surface S_B and a part on the wake surface S_W. It is representing the trailing wake propagating from the trailing edge of the body and the surface S_∞ at infinity. For an arbitrary point $\boldsymbol{X}_0 \epsilon\, \boldsymbol{\Omega}$ the potential $\boldsymbol{\Phi}$ resulting from a distribution of sources $\sigma = \sigma(\boldsymbol{X})$ and dipoles $\mu = \mu(\boldsymbol{X})$ on S_B and dipoles on S_W can be obtained by Green's third identity:

$$\boldsymbol{\Phi}(\mathbf{X}_0) = \frac{1}{4\pi}\int_{S_B \cup S_W} \mu\nabla\left(\frac{1}{d}\right)\boldsymbol{n}dS - \frac{1}{4\pi}\int_{S_B}\frac{\sigma}{d}dS \qquad [5]$$

where $\boldsymbol{n} = \boldsymbol{n}(\boldsymbol{X})$ is the normal vector of the surface element dS and $d = \|\boldsymbol{X} - \boldsymbol{X}_0\|$. For $\boldsymbol{X}\epsilon S_B \cup S_W$ holds

$$\sigma = -\nabla\boldsymbol{\Phi}\cdot\boldsymbol{n} \text{ and } \mu = -\boldsymbol{\Phi}. \qquad [6]$$

In order to obtain a physically meaningful potential and velocity field, boundary conditions have to be fulfilled on S_B, S_W and S_∞.

Fulfilling the physical Kutta condition on the wake boundary S_W in a direct way requires an iterative solution procedure. In order to simplify the calculations, Morino's Kutta condition (Morino & Kuo, 1974) is applied:

$$\mu_W = \mu_u - \mu_l \qquad [7]$$

It is based on the relation between the dipole strengths of the upper and lower side of the trailing edge and the dipole strengths of the wake surface directly behind the trailing edge.

Equation [5], combined with the above boundary conditions, results in a boundary value problem that is solved by the panel method. Hereby, the surfaces S_B and S_W are discretised by quadrilateral elements and the boundary conditions are applied at the collocation points $\mathbf{X_0}$ of each panel element. Dipoles and sources are assumed to be constant over one panel. The wake surface S_W is aligned along the streamlines of the velocity field $\mathbf{V}$ in an iterative manner in order to account for the wake roll-up. The discretised problem results in a set of linear equations for the unknown source and dipole strength, which can be solved numerically by the Gauss method.

In order to carry out a coupled simulation, the geometrically resolved propeller in the RANS simulation is replaced by a corresponding distribution of body forces. Therefore, it is necessary to map the force distribution on the blades obtained by the panel method to the volume mesh used by the RANS solver. The involved algorithm is explained in (Berger, et al., 2013). For the simulation of the propeller flow in *pan*MARE, the effective wake field is used as background flow $\mathbf{U}_\infty$. The effective wake field is approximated by subtracting the propeller-induced velocities from the total velocity field in front of the propeller which is calculated by the RANS solver.

2.2 Actuator disk

The actuator disk model is based on the approach of Manzke (2008) that refers to the numerical studies of Soukup (2008) and Xing-Kaeding (2006). The velocity distribution is taken from the current RANS solution at an axial distance of 0.05D in front of the leading edge, where D is the propeller diameter. As a modification, the local thrust for each cell volume is calculated based on the momentum theory. The modification takes the influences of the local inflow into account.

For each cell volume, the body force is set iteratively. With the inflow velocity $v_{p,local}$, a first guess of the thrust $T_{p,local}$ is derived. The local advance coefficient J_{local} for each control volume can be written as

$$J_{local} = \frac{v_{A,local}}{nD \pm \frac{v_{T,local}}{\pi}} \qquad [8]$$

with the advance velocity $v_{A,local}$ far in front of the propeller, the tangential velocity $v_{T,local}$ and the number of revolutions n, which is fixed during the iteration. The change of tangential velocity in front of the

propeller is neglected, therefore $v_{T,local}$ at the inflow plane (0.05D) is taken. The consideration of the tangential velocity is necessary to take into account the influence of the oblique inflow at the propeller location. Including data of the corresponding thrust coefficient k_T from the open water diagram according to the estimated J-value and the propeller diameter D, the initial solution is valid for the inflow velocity $v_{p,local}$ being equal to the advance velocity $v_{A,local}$.

$$T_{p,local} = \frac{k_T}{{J_{local}}^2}\rho D^2 v_{A,local}^2 \quad [9]$$

As it can be shown by momentum theory, a relation of the advance velocity to the local propeller inflow velocity can be deducted.

$$v_{A,local} = \frac{2v_{p,local}}{1+\sqrt{1+\frac{8}{\pi}\frac{k_T}{{J_{local}}^2}}} \quad [10]$$

The advance velocity $v_{A,local}$ far in front of the propeller depends on the inflow velocity $v_{p,local}$ and a value for the advance coefficient J_{local}, see Equation [10]. As shown in Equation [8], the advance velocity $v_{A,local}$ is part of the advance coefficient. Hence, an iterative solution procedure is necessary to choose the correct thrust and torque for each cell according to the local inflow.

$$T_{local} = k_T \rho n^2 D^4 \quad [11]$$

$$Q_{local} = k_Q \rho n^2 D^5 \quad [12]$$

A radial distribution r' according to Equation [13] is introduced.

$$r' = \frac{r-r_h}{r_p-r_h}\sqrt{1-\frac{r-r_h}{r_p-r_h}} \quad [13]$$

, where r_p and r_h are the propeller radius and the hub radius, respectively. The distribution is similar to the radial thrust distribution of a real propeller with its maximum near 0.7R. Near the blade tip and the propeller hub (r_h) the value of r´ is zero.

On basis of the local thrust and torque values (see Eq. [11] and [12]) multiplied with the distribution function r´, the body forces for each cell volume can be applied. After integration of the local thrust values over the propeller disk, a correction factor is needed to meet the total thrust.

2.3 Fully modelled propeller

Instead of representing the propulsor by using body forces, the flow around the propeller blades and the hub can be simulated directly with a RANS solver. The surface of the propeller is therefore discretized with triangular prism cells. A volume mesh is created around the propulsor with a refinement related to the local curvature of the blade surface. With increasing distance to the surface the mesh refinement is reduced. Obtaining the corresponding rotation rate and an inflow condition, the fluid forces on the propeller and the influence on the flow behaviour can be calculated directly in RANS simulations.

3 Case study

3.1 Geometry

The ship investigated numerically in this paper is a feeder container vessel. Initially designed within a research project at the *Potsdam Ship Model Basin*, the feeder ship is not built in full scale. Table 1 shows the main ship data. The hull is investigated in model scale and the applied scale factor is 19.2.

Table 1: Main ship data of the Feeder ship

	Full Scale	**Model Scale**
Lpp	110.0 *m*	5.73 *m*
Lwl	112.5 *m*	5.86 *m*
Bwl	18.0 *m*	0.94 *m*
T	7.1 *m*	0.37 *m*
V_{Design}	14.0 *kn*	1.64 *m/s*
V_1	10.0 *kn*	1.17 *m/s*

The ship is driven by a four-bladed controllable pitch propeller with a diameter of 4.6 *m*. Table 2 contains the main propeller data.

Table 2: Main propeller data in design condition

	Full Scale	**Model Scale**
D	4.6 *m*	0.24 *m*
Z	4	4
$P/D_{0.7R}$	0.8	0.8
Hub ratio	0.188	0.188

The model propeller has a diameter of 0.24 *m*. The pitch-diameter ratio at 0.7R is 0.8, where R is the propeller radius. The propeller rotates clockwise around the x-axis, viewed from astern. The x-axis is

directed towards the bow of the ship and is located along the symmetry plane.

3.2 Model tests

The following numerical simulations have been carried out:

- **Hull resistance test:**

The ship hull with the rudder is towed in calm water at constant ship speed.

- **Propeller open water test:**

The open water test is carried out in the towing tank, measurements are carried out at different numbers of revolutions.

- **Captive propulsion test**

The ship model is towed several times with a constant speed in calm water. Each time the propeller operates with a fixed rotation rate. The forces acting on the ship, the rudder and the propeller are measured separately. This corresponds to the British propulsion model test method.

- **Planar Motion Mechanism – Surge:**

In this test, the ship model is connected to a planar motion mechanism, which is fixed to a towing carriage. While the towing carriage moves ahead with a constant speed, the planar motion mechanism forces the ship model to perform a sinusoidal surge motion. The rudder angle and the course angle of the ship are kept zero during the test. The propeller operates with a fixed rotation rate. The results include the forces acting on the ship, the rudder and the propeller.

The sinusoidal surge motion has the amplitude A. With respect to the desired maximum surge motion amplitude and the period of the surge motion, the time-dependent surge velocity can be determined, see Equation [14].

$$\dot{x}(t) = A\omega \cos(\omega t) \qquad [14]$$

4 Numerical setup

4.1 General setup

The numerical calculations are performed using the flow solver *ANSYS CFX*. In order to represent turbulence in the near-wall and free stream region, the Shear Stress Transport model (SST) (Menter, 1992) is used. The free surface interface is modelled by the volume of fluid method (VOF) (Nichols & C.W, 1981).

All simulation are carried out with a fixed floating position with zero trim corresponding to the design waterline.

4.2 Ship Domain

The purpose of the numerical simulation of the ship flow is the calculation of the forces acting on the hull, the appendages and the propulsion device. The flow around the ship model during the captive surge motion shows a strong influence of the free surface on the estimated hull forces. Therefore, in the computations an accurate capturing of the free surface is essential to achieve a reliable estimation of hull forces. Additionally, in the numerical simulation a detailed view is given on the propulsion device and its interaction with the rudder and the hull. A fine mesh near the mentioned parts of the ship is required.

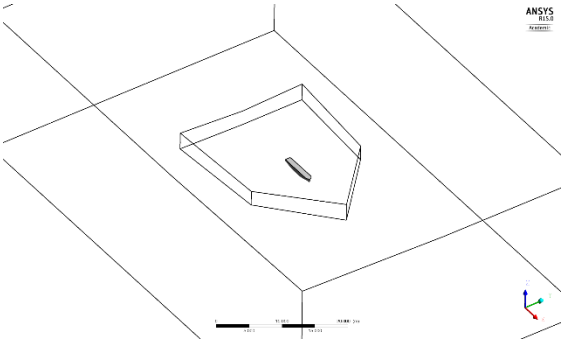

Figure 1: Topology of the computation domain

Figure 1 shows the computation domain including the ship and a subdomain to perform mesh motions, where the box around the ship moves.

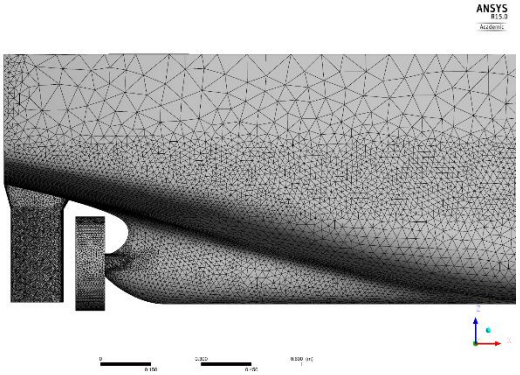

Figure 2: Aft ship with rudder and cylindrical box for the propulsor

The mesh consists of 5.4 million cells. The underwater hull surface is discretised with 26,000 surface cells, the rudder surface has 10,000 surface cells (see Figure 2). The near-wall sub-layer consists of 12 rows of prism

cells with a growth ratio of 1.1. The near-wall cell height is adapted to achieve a local non-dimensional wall distance of y^+=30.

4.3 Propeller Domain

The mesh of the fully modelled propeller consists of 2.43 million cells. Each blade is discretised with 25,000 surface cells. 12 prismatic cell layers with a growth ratio of 1.1 represent the viscous sublayer. The propeller is located in a cylindrical domain, which rotates around the center axis of the shaft (see Figure 3).

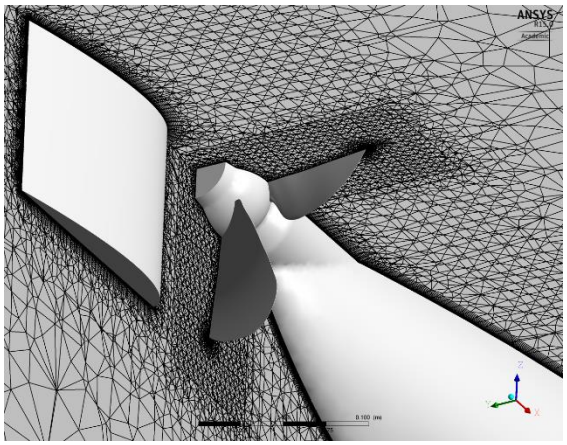

Figure 3: Mesh around the propeller and the ship stern

The domain for modelling the virtual propeller based on body forces includes 250,000 control volumes. In this domain the propeller hub is also considered. The dimensions of the cylindrical domain are similar to the fully modelled propeller domain.

5 Results

5.1 Resistance

The resistance of the ship is evaluated for the design speed V_{Desing} = 14 *kn* and for another speed V_1=10 *kn*. The resistance data can be seen in Table 3.

Table 3: Resistance data for the Feeder ship

	V [*kn*]	Model test [*N*]	Calculation [*N*]
V_{Design}	14	45.65	45.38
V_1	10	24.96	24.42

The deviation of the calculated resistance force for a full scale velocity of 14 *kn* is 0.59 % of the model test result. For V_1 the deviation is slightly larger.

5.2 Propeller open water test

The results of the propeller open water test allow a conclusion on the accuracy of forces calculated with the different propeller modelling techniques. In Figure 4, the thrust coefficient is plotted over the advance coefficient. The thrust of the fully modelled propeller (FMP) is in very good agreement with the model test results (EFD). For the range of the advance coefficients considered, the deviation of the value is in a 2%-range of the EFD results.

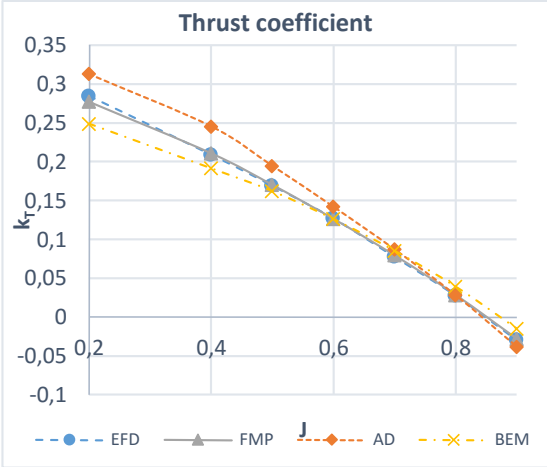

Figure 4: Thrust coefficient for the propulsion modelling techniques under open water conditions

The thrust coefficient calculated by the boundary element method (BEM) depicts a deviation for off-design advance coefficients, especially for small J-values. However, the comparison of the results to the model test results are in good agreement for a range of the advance coefficient between 0.5 and 0.8, which are within the main operating range of the propeller behind the ship.

The actuator disk model (AD) overestimates the thrust for advance coefficients less than 0.6. This may be caused by the limitation of the applicability of the momentum theory to render the induced velocities near the propeller disc (see Equation [10]).

5.3 Captive propulsion test

Captive propulsion tests offer a close insight in the interaction of the propeller, the hull and the appendages located in the propeller slipstream. A variation of the propeller load changes the flow behaviour in the aft ship region.

The numerical models are conducted to represent the propeller thrust behaviour and the local influence on

the fluid velocity distribution around the aft ship hull. All presented results are averaged over one propeller revolution.

Table 4: Total force on the ship and propeller thrust

Model	n [*rps*]	F_x Total [*N*]	Thrust [*N*]	F_x Rudder [*N*]
EFD	8	-24.62	26.57	-1.39
FMP		-24.22	27.53	-1.71
AD		-26.36	24.64	-2.34
BEM		-23.18	27.27	-2.48
EFD	8.773	-15.29	37.59	-1.60
FMP		-15.28	38.43	-1.85
AD		-15.60	36.98	-2.62
BEM		-14.29	38.14	-2.88
EFD	10	2.71	58.93	-1.85
FMP		2.36	58.84	-2.11
AD		2.44	58.29	-2.65
BEM		2.01	57.36	-3.61

Table 4 includes the propeller thrust and the total forces in the local x-direction for 3 different rotation rates and V_{Design}. The total force includes the ship resistance, the rudder resistance as well as the propeller thrust. The results of the fully modelled propeller case (FMP) are in good agreement with the EFD for the towing force and the thrust. The actuator disk model (AD) underestimates the thrust. It leads to a slightly lower thrust and therefore a larger towing force.

For higher rotation rates of 8.773 *rps* and 10 *rps* the modelling techniques FMP and AD lead to results that are very close to the EFD results. For the rotation rate of 10 *rps*, the propeller thrust is higher than the resistance of the ship and the rudder, which leads to a positive total force.

Furthermore, Table 4 shows the forces on the rudder in the x-direction. For all evaluated operating conditions, the resistance force of the rudder is overestimated in the numerical simulations. The usage of the FMP leads to a less over prediction compared with AD and BEM coupling.

For further understanding of the influence of the propulsion modelling on the local flow state behind the propulsion device, the averaged velocity distribution is focused now at a location 0.25D downstream of the propeller center. In Figure 5, the local velocities behind the propeller are shown.

The maximum axial velocity is 2.21 *m/s* for the FMP and 2.35 *m/s* for the AD, whereas the average velocity is almost similar for both cases (AD: 1.41 *m/s*, FMP: 1.45 *m/s*). The contours of the velocity component in the y-direction (middle figure) at the 12 o'clock position are more pronounced in the FMP case. Higher velocities in the y-direction lead to a higher angle of attack at the rudder resulting in a lift force. The increase of the angle of attack leads to a proportional increase of the lift force. This force acts against the resistance force. The velocity distribution in z-direction is mainly quite similar and seems to have no

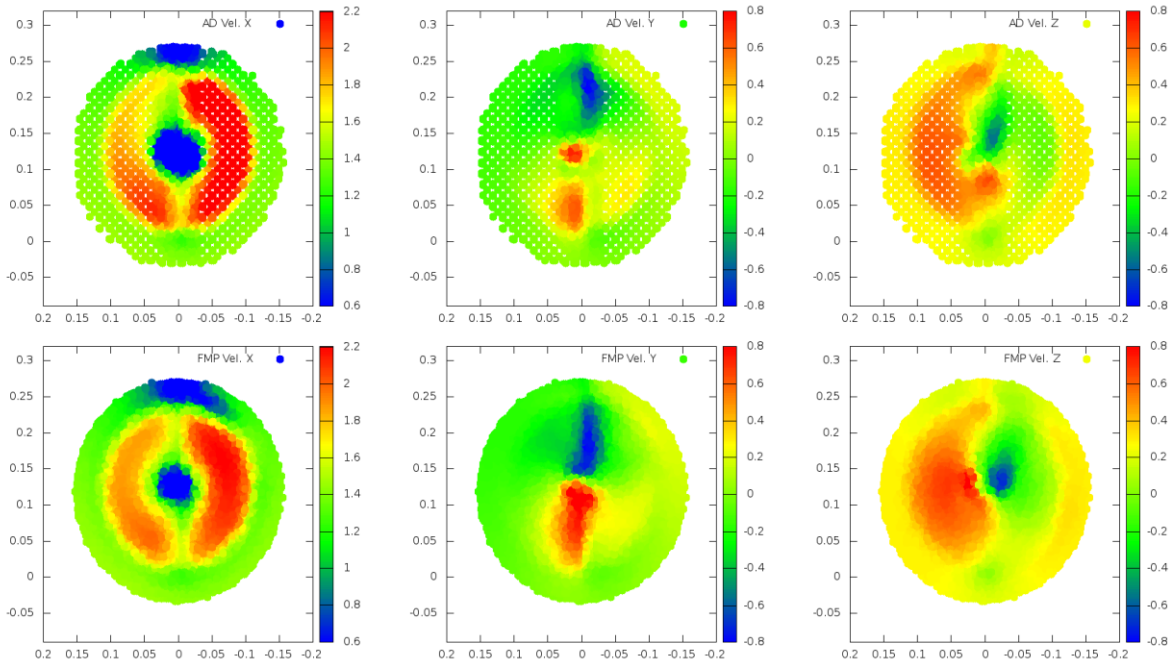

Figure 5: Averaged velocity distribution in [m/s] 0.25D behind the propeller for the AD case (upper row) and the FMP case (lower row), rotation rate of 10 rps, ship speed 14 kn in full scale

significant effect on the forces acting on the rudder. For lower rotation rates the differences in the distributions are smaller, but they show the same tendency as presented in Figure 5.

A comparison of the BEM coupling with the FMP case for a rotation rate of 10 *rps* is shown in Figure 6. The velocity distributions are quite similar. The maximum velocity in axial direction is with a value of 2.32 *m/s* higher than the 2.21 *m/s* in the FMP case. The average axial velocity behind the propeller is with a value of 1.37 *m/s* lower than in the FMP case.

A more detailed view on the influence of the propeller on the flow behaviour can be seen in Figure 7. The velocity distribution in a distance of 0.25D in front of the propeller (upstream) is compared to the flow behaviour 0.25D behind the propeller (downstream) for the three modelling techniques. The given angle describes the location of the blade during a rotation of the propeller. An angle of 0° corresponds to the 12 o'clock position. The values shown in the following figures are averaged over one revolution of the propeller.

With a rotation rate of 10 rps at a ship speed of v_{Design}=14 *kn*, the fluid approaches the propeller with around 90% of the design speed between 60° and 300°. The reduction of the axial velocity at an angle of 0° is typical for a wake field of a ship with a single screw. The propeller accelerates the fluid to a velocity 30% higher than the ship speed, with a reduction at 0° and 180° due to the influence of the rudder.

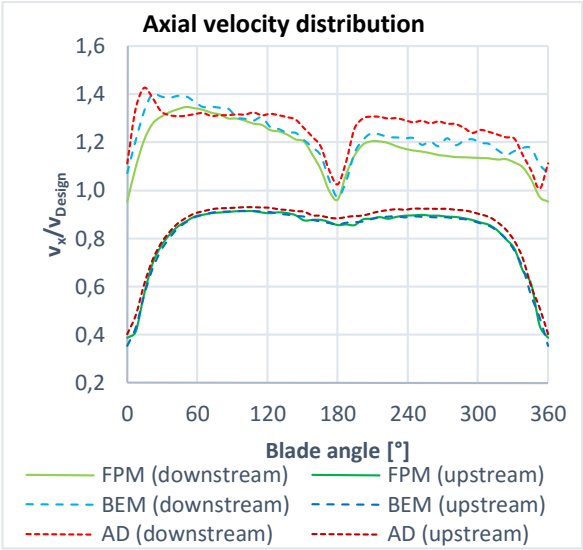

Figure 7: Velocity in axial direction in front of and behind the propeller on 0.7R (10 *rps*, V_{Design})

Caused by a general upward flow upstream of the propeller, the radial velocity distribution in Figure 8 is mainly influenced by the vertical velocity, working in a negative radial direction for blade angles between 90° and 270°. The velocity distribution behind the propeller indicates a contraction of the slip stream for the mentioned range of angles, resulting in negative radial velocities. For blade angles between 300° and 60°, the rudder induces a velocity directed outward, leading the flow around the rudder. Due to a high thrust loading in the range between 0° and 60°, a large deviation between the results of the three applied methods can be observed downstream of the propeller.

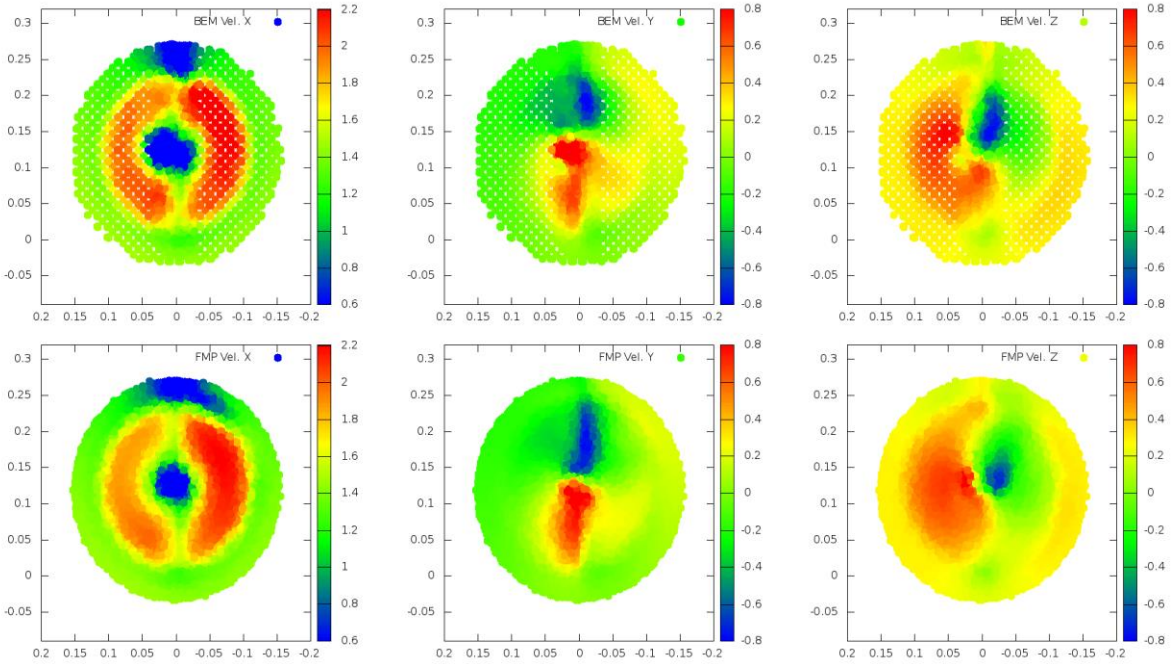

Figure 6: Averaged velocity distribution in [m/s] 0.25D behind the propulsion device for the BEM case (upper row) and the FMP case (lower row), rotation rate of 10 rps, ship speed 14 kn in full scale

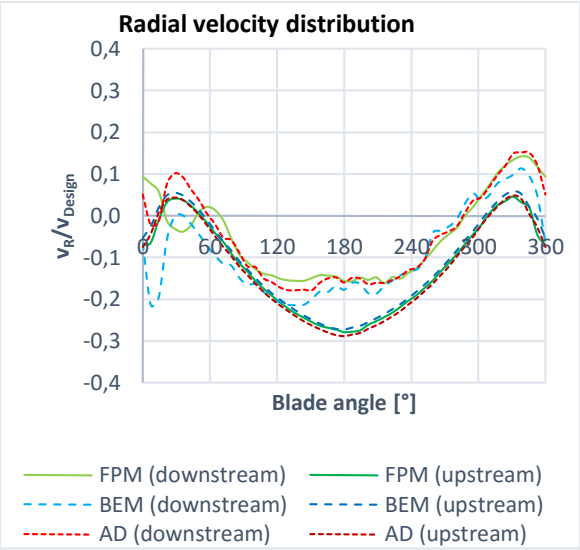

Figure 8: Velocity in radial direction in front of and behind the propeller on 0.7R (10 *rps*, V_{Design})

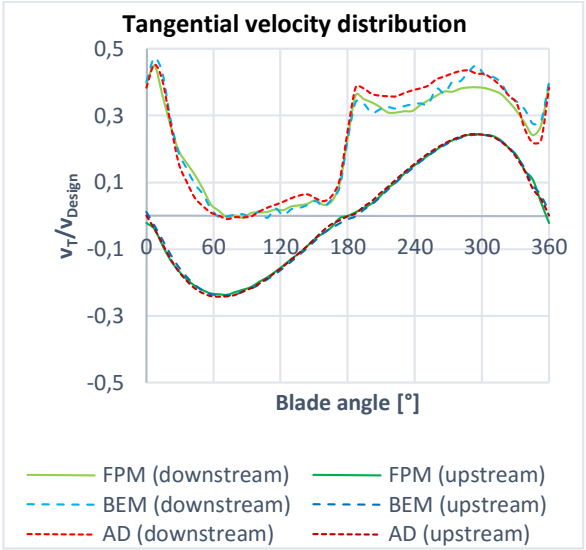

Figure 9: Velocity in tangential direction in front of and behind the propeller on 0.7R (10 *rps*, V_{Design})

The tangential velocity distribution does not indicate any significant differences, see Figure 9. Thus, the deviation of the rudder resistance force in Table 4 cannot be explained by different tangential velocities. The velocity distribution indicates a symmetric inflow to the propeller. For angles in a range between 60° and 180°, the propeller benefits from the pre-swirl energy. As a result, the advance coefficient in Equation [8] decreases, which leads to an increase of the local thrust.

Due to the contrary direction of the fluid and the propeller blades, the resulting vertical velocity downstream of the propeller is zero. For blade angles larger than 180°, the propeller blades produce a swirl with the same orientation as the tangential flow velocity in front of the propeller. The advance coefficient increases. The pre-swirl and the rotational loss of the propeller have the same direction of rotation and results in a large tangential velocity.

In Figure 7 and Figure 9 in a range between 180° and 360°, the AD model overestimates the axial velocity and tangential velocity components downstream of the propeller, compared to the FMP and BEM cases. Thus, the local effect of the tangential velocities on the fluid acceleration by the propeller is not sufficiently captured by the AD model.

5.4 Planar Motion Mechanism – Surge

The capability of the actuator model for dynamic tests is demonstrated exemplarily for surge motion.

In the planar motion test, the ship is running ahead with a velocity of 14 *kn*. Then, the ship is forced to perform a surge motion as shown in Figure 10. The time 0 *s* indicates the start of a surge period. Referring to Equation [14] the maximum change of the ship's speed relative to the fluid velocity is 0.235 *m/s* (corresponding to full scale velocity: 2 *kn*).

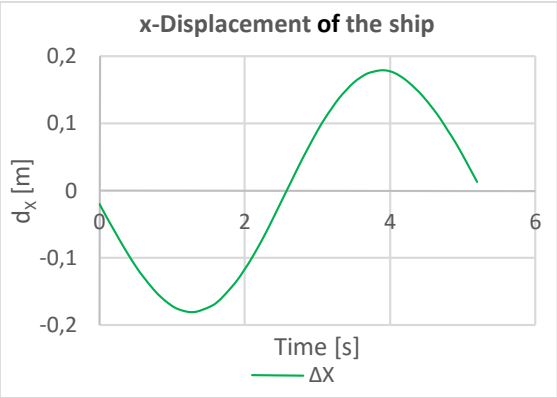

Figure 10: x-Displacement of the ship under planar surge motion conditions

The force in x-direction is not symmetric in Figure 11, because it is shifted by the steady ship resistance component. The propeller model operates in an oscillating inflow velocity field and thus causes a periodical change of the rudder resistance, see Figure 12.

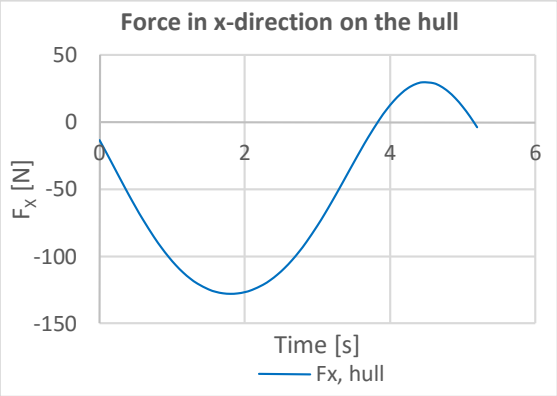

Figure 11: Force in x-direction on the ship hull under planar surge motion conditions

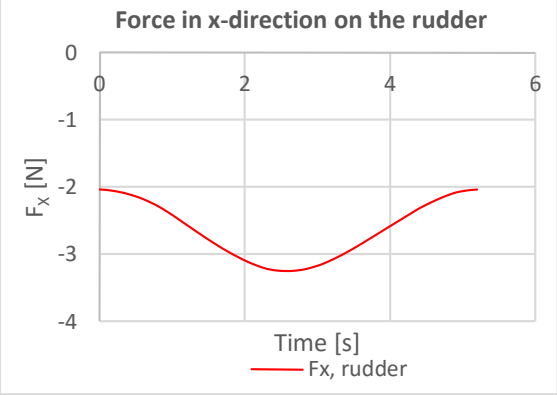

Figure 12: Force in x-direction on the rudder under planar surge motion conditions

The maximum rudder force shown in Figure 12 occurs at around 2.5 *s*. That instant of time is in accordance with the maximum value of the thrust in Figure 13.

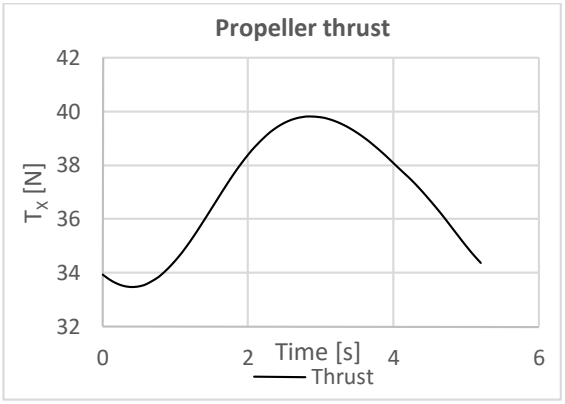

Figure 13: Propeller thrust under planar surge motion conditions

6 Conclusion

The captive propulsion test allows the evaluation of the applicability of the different propulsion modelling techniques for simulation of ship manoeuvres. The propeller modelling techniques applied in the paper are able to capture the propeller forces and the flow behaviour around the aft-ship and the rudder.

Where, over the investigated range of propeller loading conditions, the results of the fully modelled propeller show a good agreement with the measured values. The results of the actuator disk and the BEM coupling method are in good agreement with the experimental results only for advance coefficients close to the design condition.

For lower propeller loading conditions, the actuator disk model generates a significantly less thrust than the measured value. The BEM coupling method is generally in good agreement with the measured results and the computation time is much less than the time required for simulation with a fully modelled propeller.

The application of the actuator disk model for planar motion surge mechanism simulations delivers realistic results and much less computation time is required, compared with the other two simulation techniques.

7 Acknowledgement

The work presented in this paper is part of the tasks to be executed in the research project “OptiStopp”. The research project is supported by the Federal Ministry

of Economic Affairs and Energy of Germany. The aim of the project is to simulate stopping manoeuvres using time-efficient system based methods. The project partners are *Thyssen Krupp Marine Systems GmbH*, *SVA Potsdam GmbH* and *Siemens AG*.

8 References

Berger, S., 2011. *Kopplung eines Rechenverfahrens für potentialtheoretische Strömungen mit einem Rechenverfahren für viskose Strömungen mit Hilfe eines Propellermodells.* Hamburg: Hamburg University of Technology.

Berger, S., Bauer, M., Druckenbrod, M. & Abdel-Maksoud, M., 2013. *An Efficient Viscous/Inviscid Coupling Method for the Prognosis of Propeller-Induced Hull Pressure Fluctuations.* Launceston, Australia: Third International Symposium on Marine Propulsors smp'13.

Bugalski, T. & Hoffmann, P., 2011. *Numerical Simulation of the Self-Propulsion Model Tests.* Hamburg, Germany: Second International Symposium on Marine Propulsors smp'11.

Greve, M., Abdel-Maksoud, M., Eder, S. & De Causmaecker, J., 2010. *Unsteady Viscous Flow Calculation around the KCS-model with and without Propeller under consideration of the Free Surface.* Gothenburg, Sweden: Proceedings of Workshop on Numerical Ship Hydrodynamics Gothenburg 2010.

Krasilnikov, V., 2013. *Self-Propulsion RANS Computations with a Single-Screw Container Ship.* Launceston, Australia: Third International Symposium on Marine Propulsors smp'13.

Manzke, M., 2008. *Numerical Simulation of Unsteady Body Motion in Turbulent Flow.* Hamburg: Hamburg University of Technology.

Menter, F., 1992. *Improved two-equation k-omega turbulence models for aerodynamic flows.* Moffett Field, California, USA: NASA Technical Memorandum.

Morino, L. & Kuo, C., 1974. *Subsonic potential aerodynamic for complex configrations: a general theory.* Boston, USA: AIAA Journal, Vol. 12, No. 2.

Nichols, B. & C.W, H., 1981. *Volume of fluid (VOF) method for the dynamics of free boundaries.* Los Alamos, New Mexico, USA: Los Alamos Scientific Laboratory.

Rijpkema, D., Starke, B. & Bosschers, J., 2013. *Numerical simulation of propeller-hull interaction and determination of the effective wake field using a hybrid RANS-BEM approach.* Launceston, Australia: Third International Symposium on Marine Propulsors smp'13.

Soukup, P., 2008. *Report on Free Running Model Simulation for Steady Turning.* Hamburg: Hamburg University of Technology.

Tian, Y. & Kinnas, S., 2012. *A Wake Model for the Prediction of Propeller Performance at Low Advance Ratios.* Austin, Texas, USA: University of Texas.

Wöckner, K. et al., 2011. *Unsteady Viscous/Inviscid Coupling Approaches for Propeller Flow Simulations.* Hamburg, Germany: Second International Symposium on Marine Propulsors.

Xing-Kaeding, Y., 2006. *Unified Approach to Ship Seakeeping and Manoeuvring by a RANSE Method.* Hamburg: Hamburg University of Technology.

9 DISCUSSION

9.1 Question from Sverre Steen

The title of the paper mentions manoeuvring, and in the introduction part of the presentation you state that crashback is the ultimate aim of your work, while what you present here is just straight ahead. How do you plan to address the complicated, separated flow of the crashback condition?

9.2 Authors' Closure

Thank you for your observation. The crashback situation with the propeller acting opposite to the general flow direction is indeed a highly complicated case. Since the general approach using the actuator disk model based on the momentum theory is not valid for off-design cases, a specification containing a prescribed thrust and torque and a distribution factor for a tangential distribution will be implemented. Based on a few simulations for flow conditions occurring during a crashback manoeuvre with a fully-modelled propeller, the prescribed input values for the actuator will be interpolated and the coefficients for the off-design conditions can be calculated.